Digest Journal of Nanomaterials and Biostructures Vol. 6, No 2, April - June 2011, p. 523 - 534

SYNTHESIS, MECHANICAL AND STRUCTURAL PROPERTIES AND BIOLOGICAL ACTIVITY OF SOME NANOSTRUCTURED BONE SCAFFOLDS

C. VASILESCU[a*], J. M. CALDERON MORENO[a], A. CIMPEAN[b], D. COJOCARU[c], I. CINCA[c], E. ANDRONESCU[c], F. GRIGORE[d], B. GALATEANU[b], S. I. DROB[a]

[a]*Institute of Physical Chemistry "Ilie Murgulescu", Spl. Independentei 202, 060021, Bucharest, Romania*

[b]*Department of Biochemistry and Molecular Biology, University of Bucharest, Spl. Independentei 91-95, 050095, Bucharest, Romania*

[c]*Politehnica University of Bucharest, Spl. Independentei 313, 060042 Bucharest, Romania*

[d]*National Research Institute for Electrical Engineering, Spl. Unirii 313, 030138 Bucharest, Romania*

Three new biodegradable and bioactive scaffolds based on hydroxyapatite (HAP), β tricalcium phosphate (β-TCP) and a composite HAP+β-TCP are studied in this paper. Their mechanical, structural properties and long term behaviour in simulated body fluid (SBF) were analysed. Also, these scaffolds were subjected to *in vitro* evaluation of cell behaviour. The open porosity from 16.41% to 34.26% it resulted. The compression resistance (2-3 MPa) is very close to the cancellous bone. It resulted that simultaneously with the dissolution, on the surface of materials were deposited calcium and phosphorous ions, namely, these materials are favourable to the bone formation. The scaffold morphology showed a dense polycrystalline structure with cavities (porosity), junctions and interconnections that can facilitate the cell proliferation. SEM micrographs revealed that, after 2100 immersion hours in SBF, the scaffolds coated with a layer of micro-sized grains. The *in vitro* results proved that hFOB 1.19 cells are able to attach, migrate in the interior of scaffolds, proliferate, synthesize and extracellularly assemble ECM molecules.

(Received February 4, 2011; March 9, 2011)

Keywords: Nanostructure, Porosity, Scaffolds-biofluid interactions, *in vitro* cell behaviour, SEM

1. Introduction

A scaffold with applications in bone tissue engineering has to be biocompatible, osteoinductive and able to withstand mechanical loading [1-3]. Also, the scaffolds have to fulfil few main requirements: high porosity and proper pore size, required surface properties permitting cell adhesion, differentiation and proliferation, desirable mechanical integrity to maintain the predesigned tissue structure and non-toxicity [4-9].

An important parameter for the scaffold is its porosity [10] which should facilitate the migration and proliferation of precursor cells, provide an appropriate microenvironment for cell proliferation and differentiation and allow for the mass transfer of nutrients, oxygen and waste within the construct [10-12]. Higher porosities result in greater bone ingrowths *in vivo* but in a lower mechanical strength; so, the porosity of the scaffold must lie within a critical range, small enough to maintain its mechanical integrity and large enough to provide optimal bioactivity. It was

* Corresponding author: cora_vasilescu@yahoo.com

proved [13,14] that pores with a diameter between 50 μm and 150 μm can lead to the formation of mineralized bone directly.

The degree of the interconnectivity [15,16] of pores is very important for the success of an implant. But, conflict interests exist between biological and mechanical requirements, thus the design of a porous implant material with a sufficient degree of interconnected porosity combined with optimal mechanical properties is an important challenge.

Another property is the balance between the rate of bone remodelling and the rate of degradation of scaffold [15,17,18]. A good scaffold must be biodegradable such that it has to be gradually replaced by growing bone tissue [19]. A progressive increase of the deposited new bone throughout the open pore structure of the scaffold together with a reduction in the resorption quantity of the scaffold material and its subsequent replacement with highly mineralized lamellar bone are interrelated and necessary for the normal bone remodelling process [19,20].

Hydroxyapatite [1,21,22] has a composition and structure very close to natural bone mineral but its poor brittleness and mechanical stability limit its use.

Calcium phosphates in amorphous and crystalline form [2,15,23,24] play a critical role in the process of the tissue mineralization: it is a precursor of other crystalline phases, in the early stage of tissue mineralization; it is a temporary storage for Ca and P sources.

Despite extensive researches, no existing scaffold can meet all necessary requirements for every good scaffold. The development of novel biomaterials and scaffold fabrication techniques is critical for the success of the bone tissue engineering [25,26].

Three new biodegradable and bioactive scaffolds based on hydroxyapatite (HAP), β tricalcium phosphate (β-TCP) and a composite of hydroxyapatite (50% HAP) + β tricalcium phosphate (50% β-TCP) labelled as HAP+β-TCP are studied in this paper. Their mechanical and structural properties and long term behaviour in simulated body fluid (SBF) were analysed. Also, these scaffolds were subjected to *in vitro* evaluation to assess the cell behaviour in terms of cell viability, morphology and adhesion.

2. Experimental

Scaffold obtaining

Ceramic powder obtaining. Synthesis of ultra-fine powders of hydroxyapatite and tri-calcium phosphate was realized by precipitation from salted solutions $(NH_4)_2HPO_4$ and, respectively, Ca $(NO_3)_2$.$4H_2O$ (Merck). The purpose was the obtaining of three powder categories with particles average dimension of 200 μm maximum:

- ceramic powder with majority phase of β – tricalcium phosphate (β-TCP);
- ceramic powder with majority phase of hydroxyapatite (HAP);
- bi-phase ceramic powder: 50% β-TCP + 50% HAP (HAP+βTCP).

During of the synthesis procedure, main parameters have been maintained as follows: high purity raw materials used for synthesis; the temperature of homogenization was between 30^0-50^0C; pH level was maintained between 7 and 10; the calcinations temperature, maximum 850^0C for β-TCP, and maximum 1100^0C for HAP [27].

In Figure 1 is indicated the diagram of procedures which has been applied in purpose to obtain the three different types of ceramic powders.

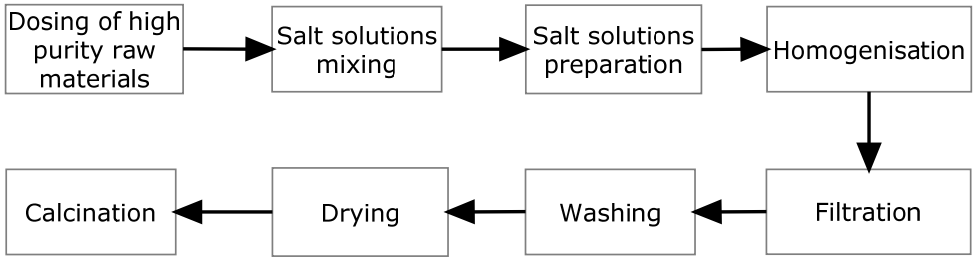

Fig. 1. Obtaining procedure for the ceramic powders (schematic diagram)

Preparation of the ceramic suspensions. Obtaining of ceramic product with high qualitative performances has implied preparation of a stabile suspension, with high powder content and with rheological properties which permit the impregnation of polyurethane foam. Characteristics of suspensions which has been obtained and used till present are the following: 70% ceramic powder; distilled water as dispersion medium; ~2% sodium polyacrylate as dispersant; 0,6% polyethylene oxide as binder.

These suspensions have a pseudo-plastic character, with registered values of beta potential between -17 mV and -60 mV, and viscosity values under 7 Pas. Optimal variant of stable suspension elaboration, with a phosphate powder content of 70%, was realized by powder mixing and homogenization in a mill with balls, together with medium of dispersion, the dispersant and, respectively, the binder. In the first step, organic dispersant (~ 2% sodium polyacrylate) has been dissolved in distilled water, after which the powder was added, with a first homogenization of 30 min. The binder (0.6% polyethylene oxide) was added at end, after which the homogenization was continued in ball-mill during 2 h.

Scaffold obtaining. For the scaffold obtaining, the technique of replication [27] was applied: in a first step, an impregnation of the polymeric porous material (the porous dimension between 150-500 μm) with ceramic suspension, which contains dispersant and surfactant was carried out. Impregnation was made by a simple immersion in suspension. After impregnation, the sponge was compressed using a rolling system in order to eliminate the excess ceramic suspension and to realize a homogeneous distribution in the polymeric structure. Drying was made in air, during 24 hours, and then in the drying stove at 60^oC for 8 hours. In order to eliminate the polymeric support, the sponge, impregnated with ceramic suspension, was heated very slowly until 550^oC (temperature selected according polymer nature). Sintering was made at 1000^oC, with 2 hours of maintaining.

Scaffold characterisation

Determination of compression resistance. Tests of compression resistance were carried out on Material Testing Machine - Zwick. Three samples of 1x1.5x3 cm dimensions for each determination were used and the reproducibility was very good.

Porosity characterisation. The open porosity was determined with a mercury porosimeter type Pascal 140/240, which can measure pores with a diameter till 3.7 nm.

Determination of scaffold morphology. The microstructure of the scaffolds before and after immersion (2100 hours) in simulated body fluid (SBF) was investigated by scanning electron microscopy (SEM) using a EVOLS10 electron microscope operated at accelerating voltage of 15 kV [28,29]. SEM observations determined the three-dimensional structure of the scaffolds, the porosity, particle size and thickness of the scaffolds walls, and the surface evolution with the time after the immersion in SBF.

Interactions of scaffolds with biofluid. Simulated body fluid (SBF) had the composition (g/L): NaCl – 7.99; KCl – 0.224; $NaHCO_3$ – 0.35; $K_2HPO_4 \cdot 3H_2O$ – 0.228; $MgCl_2 \cdot 6H_2O$ – 0.305; $CaCl_2$ – 0.278; Na_2SO_4 – 0.071. Temperature was kept at $37^0 \pm 1^0C$.

The following experimental techniques were used: monitoring of scaffold weight, of SBF *p*H, analysis of the calcium and phosphorous ions content by induced coupled plasma–optical emission spectroscopy (ICP-OES) and the study of the scaffold morphology using scanning electron microscopy (SEM).

For the monitoring of weight, the samples were exposed for long term (3000 hours) in SBF and were periodically verified. Evaluation of the weight was made by the determination of the percentage variation of the weight after immersion in SBF:

$$\Delta G = \frac{G_2 - G_1}{G_1} \cdot 100$$

where: G_1 is the initial weight of the sample and G_2 is the sample weight after immersion in biological fluid and drying in air for about 2 hours (till a constant weight is reached). Negative values for ΔG show the weight loss, i.e., the material is dissolved in SBF. Positive values of ΔG show ion deposition from SBF.

Variation of *p*H values of the simulated body fluid for long term was carried out with a pH-meter InoLab WTE (Germany) with a precision of ±0.01.

Induced coupled plasma–optical emission spectroscopy (ICP-OES, Perkin Elmer) was used for to determine the long term change (3000 hours) of the calcium and phosphorus ion quantity, so monitoring these ions deposition on the scaffolds.

In vitro evaluation of cells behaviour

Osteoblast cell culture. Human fetal osteoblasts (hFOB 1.19, purchased from American Type Cell Culture Collection) were cultured in DMEM-Ham's F-12 1:1 media (Sigma-Aldrich) supplemented with 10% fetal bovine serum (FBS, Gibco) and 0.3 mg/ml G 418 antibiotic, and incubated at 34ºC in a humidified atmosphere with 5% CO_2. The culture medium was changed every third day [30]. Cells were detached by treatment with trypsin–EDTA (0.25% and 0.03%, respectively) and seeded, at a final density of 5 x 10^4 cells/cm^2, on each disc-shaped scaffold, placed in 24-well plates and maintained in standard culture conditions up to 10 days.

Cytotoxicity assay of scaffolds toward hFOB 1.19 cells. The potential cytotoxicity of the three ceramic supports was assessed by measuring lactate dehydrogenase (LDH) leakage of hFOB 1.19 cells into the culture medium. Samples of 100 µL culture media were taken at 24 and 96 hours post-seeding and a LDH test was performed by using Cytotoxicity Detection Kit (TOX-7, Sigma) according to the manufacturer's protocol. Data are presented as the average of three replicates (mean ± standard deviation).

Fluorescence microscopy. Cells were fixed for 15 min at room temperature (RT) in 4% paraformaldehyde. After washing in PBS, cells were then routinely processed for fluorescent labelling. Briefly, they were permeabilized with 0.1% Triton X-100 in PBS for 15 min., followed by blocking with 2% bovine serum albumin in PBS for 1 h. For β1-integrins labelling, cells were not permeabilized. Primary antibodies to β1-integrins and fibronectin (Fn) were used, followed by corresponding fluorescein isothiocyanate (FITC)-conjugated secondary antibodies (Santa Cruz Biotechnology), or by tetramethyl rhodamine isothiocyanate (TRITC)-conjugated secondary antibodies, diluted 1:100 in PBS. All incubations were performed in a humidified environment for 2 h at RT, followed by three 5 min washes in PBS. For actin visualization, the samples were incubated for 1 h at 37ºC with FITC-conjugated phalloidin. The nuclei were counterstained with 2 µg/mL DAPI (Sigma) for 10 min. Samples were examined under a fluorescence microscope Olympus IX71 and the images were captured and processed with Cell F software. Triplicate culture experiments were performed.

3. Results

Compression resistance of the scaffolds. The compression resistance of the studied scaffolds (Table 1) varied around 2-3 MPa, very close with of the cancellous bone [3].

Table 1. Values of the compression resistance (R_m) of the scaffolds

Parameter	Type of scaffold		
	HAP	β-TCP	HAP+β-TCP
Rm (MPa)	2.89	2.64	2.77

R_m – mechanical resistance to compression

Scaffold porosity varied in normal limits [2] from 16.41% to 34.26% (Table 2).

Table 2. Porosity of the analysed materials

Sample	Average dimension of the pores (µm)	Open Porosity (%)
β-TCP	2.98	16.41
HAP	0.25	34.26
HAP+β-TCP	0.61	21.70

The ceramic material based on HAP have the most high value of open porosity but with smaller pores, and the ceramic composite (HAP+β-TCP) have average values of this two

characteristics. The curves of the dimension distribution of the pores are presented in Figure 2 and show bimodal or three modal distribution [22] with the following observations:
- for HAP scaffold, the curve of dimension distribution revealed a three modal distribution, with pores of dimensions from 0.05 μm to 100 μm;
- for β-TCP scaffold, the dimension distribution of pores comprises two modes, with maxima at 0.05 μm – 10 μm and 50 μm – 100 μm;
- for composite HAP+β-TCP scaffold, the pore dimensions have two maxima in the range: 1 μm – 5 μm and 50 μm – 100 μm.

The composite scaffold (HAP+β-TCP) has the open porosity values and average pore dimension values between corresponding values of HAP and β-TCP scaffolds.

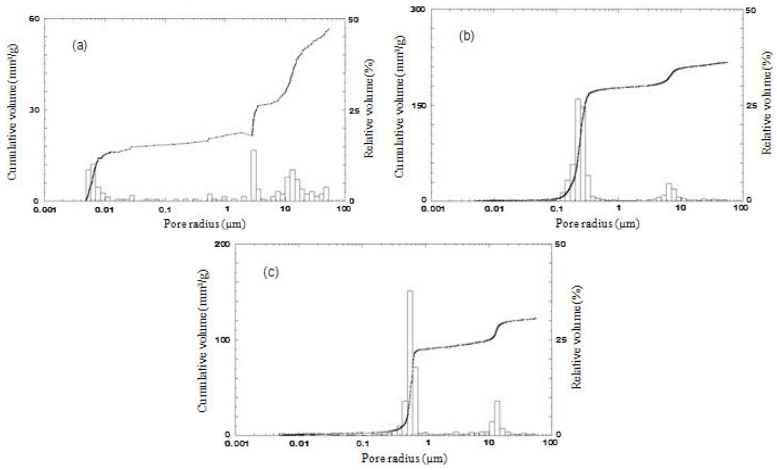

Fig. 2. Distribution of pore dimensions for: a) HAP; b) β-TCP; c) HAP+β-TCP

Scaffold morphology. The initial SEM images in Figure 3 revealed the sponge-like architecture of the three as-prepared scaffolds HAP (Fig. 3A-B), β-TCP (Fig. 3C-D) and HAP+β-TCP (Fig. 3E-F). All the scaffolds show an open three-dimensional network of interconnected cavities, randomly oriented. The cavities are round-shaped, in the micro-size range, with typical diameters of a few hundred microns. The surfaces of the cavities walls were observed at higher detail (Fig. 3B-D-F), showing in all the scaffolds a nearly dense polycrystalline microstructure typical of sintered powders, with some residual isolated porosity at triple points and grain junctions and homogeneous grain sizes. Grain sizes of the walls are about 3-4 μm in β-TCP (Fig. 3D) and HAP+β-TCP (Fig. 3F) scaffolds, and smaller, below 1 μm, in HAP (Fig. 3B).

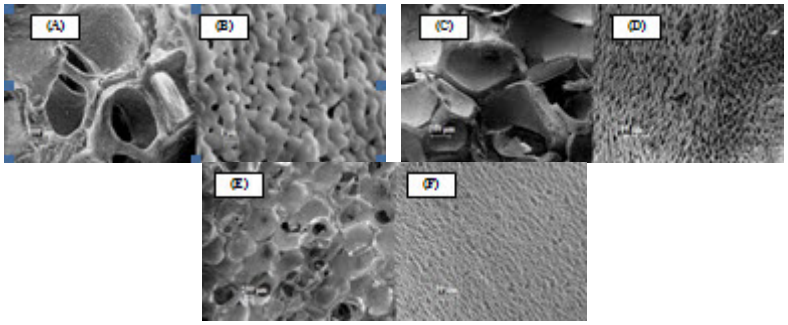

Fig. 3. SEM micrographs illustrating the initial scaffold structures and the surface of the walls: (A-B) HAP; (C-D) β-TCP; (E-F) HAP+β-TCP

Long term interactions of scaffolds with SBF

Interactions of scaffolds with SBF from weight variations. From Table 3 it resulted a different behaviour of the studied scaffolds: the weight of the HAP scaffold increased in time; the weight of β-TCP scaffold decreased in time and of the HAP+β-TCP scaffold decreased with a lower rate than of the β-TCP scaffold.

Table 3. Weight variations (ΔG) of scaffolds.

Material	ΔG (%) after				
	700 h	1100 h	1600 h	2200 h	3000 h
HAP	5.92	8.12	8.25	8.27	8.20
β-TCP	-1.34	-1.56	-1.65	-2.20	-2.94
HAP+β-TCP	0.32	-0.09	-0.66	-0.97	-1.59

Interactions of scaffolds with SBF from pH variations. The pH values (Fig. 4a) of simulated body fluid had the same variations in time (3000 immersion hours) for the three studied materials: an increase in the first 500 hours, a slow decreasing till 1000 hours and then an about constant level up to 3000 immersion hours.

Interactions of scaffolds with SBF from the monitoring of calcium and phosphorous ion quantity. The quantity of calcium (Fig. 4b) and phosphorous (Fig. 4c) ions from SBF decreased in time for 1000 immersion hours due to their deposition on the scaffolds surface. After 1000 immersion hours, their concentrations remained about constantly, i.e., the simultaneous processes of dissolution and deposition reached an equilibrium, were compensated.

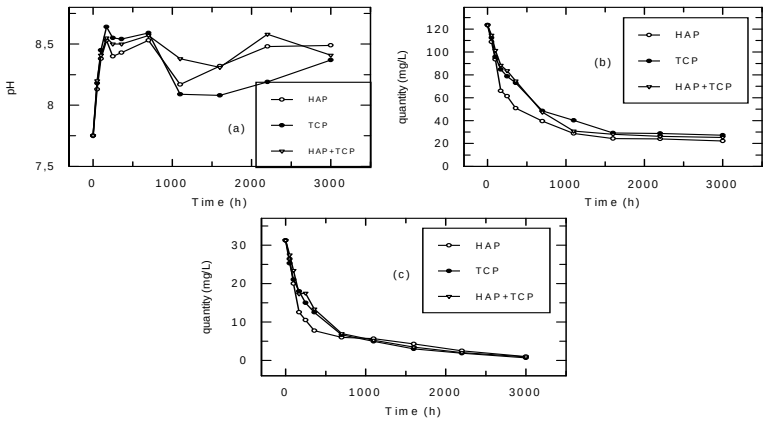

Fig. 4. Variation of: a) pH; b) calcium ion quantity; c) phosphorous ion quantity

Long term morpho-structural changes of the scaffolds

The SEM images in Figure 5 show the scaffolds structure and surface changes after immersion in simulated body fluid (SBF) for 700 h for HAP (Fig. 5A-B), β-TCP (Fig. 5C-D) and HAP+β-TCP (Fig. 5E-F). The macroscopic appearance of the scaffolds: the cavities shape, size and overall morphology are retained**.** The higher detail study of the wall surfaces (Fig. 6A-B) revealed significant modifications: the grain junctions and triple points appear masked and most nano-sized pores are fully or partially covered by a surface layer, increased roughness and reduced porosity in the walls are clear in all the scaffolds. Immersion in SBF for 700 h also resulted in the scattered deposition of aggregates of acicular grains in the β-TCP scaffold (Fig. 6C-D). Also, the HAP scaffolds showed a characteristic feature after immersion in SBF, namely the growth of web-like structures (Fig. 6E-F). Neither nano-particle aggregates nor web-like structures are observed in HAP+β-TCP scaffold after 700 h immersion.

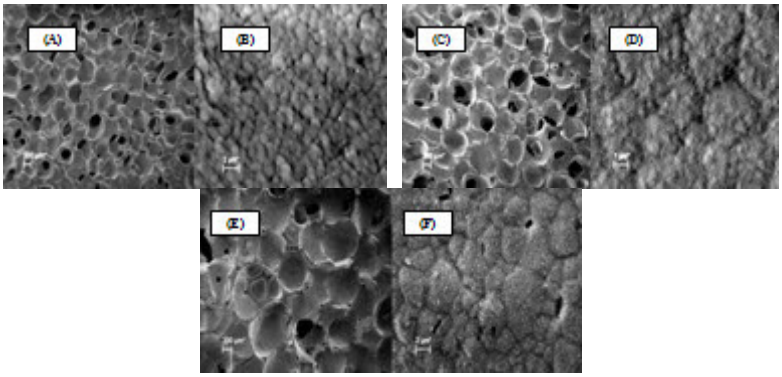

Fig. 5. SEM micrographs showing the scaffold structures and the surface of the walls after immersion in SBF for 700 h: (A-B) HAP; (C-D) β-TCP; (E-F) HAP+β-TCP

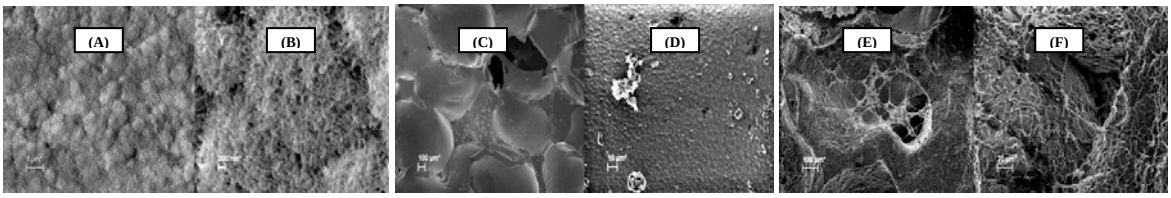

Fig. 6. SEM micrographs with: (A-B) nano-sized acicular grains on HAP; (C-D) deposition of aggregates of acicular grains on β-TCP; (E-F) growth of web-like structures between walls in the HAP scaffolds after immersion in SBF for 700 h

Immersion for 2100 h resulted also in the coating of the walls with a layer of nano-sized acicular grains on all three materials. The distinctive features of web-like structures connecting long thin filaments, grown from the wall surfaces, are clearly observed in HAP after 2100 h immersion (Fig. 7A). The web-filaments can reach lengths of several millimetres. Such web-like structures does not grow on β-TCP, neither on HAP+β-TCP. On β-TCP walls, additionally to the nano-filaments surface layer, observed in all the scaffolds, additional aggregates of deposited nano-particles are ubiquitous, covering areas of hundred of microns (Fig. 7B). Similar aggregates can be also observed on HAP+β-TCP after 2100 h immersion (Fig. 7C).

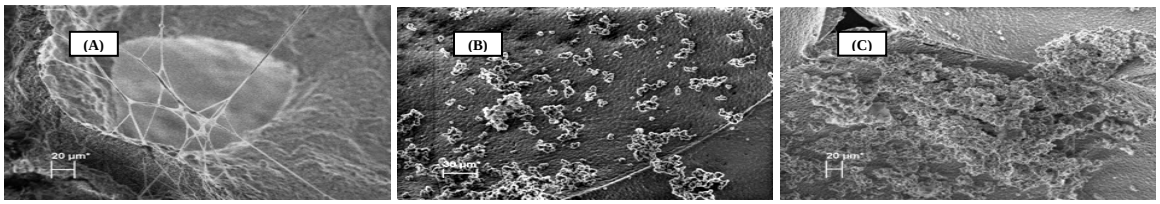

Fig. 7. SEM micrographs showing the scaffolds: (A) HAP; (B) β-TCP; (C) HAP+β-TCP after immersion in SBF for 2100 h

In vitro cell behaviour on the scaffold surfaces

LDH cytotoxicity assay. The cytotoxicity (cell viability) of the cells grown in contact with the three analyzed scaffolds was assessed by the LDH assay. By analyzing the obtained results (Fig. 8), it was noticed that all three scaffolds displayed low LDH release in culture medium, suggesting that none of these materials exerted cytotoxic effects.

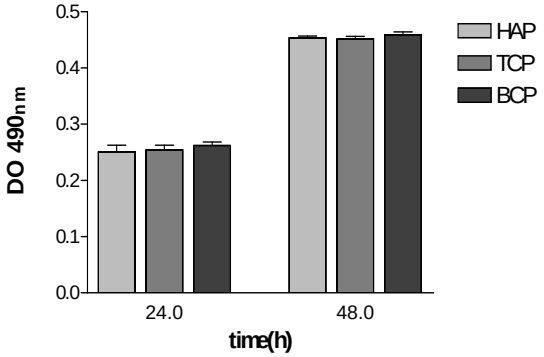

Fig. 8. Representation of graph showing the LDH release in culture media from bioceramic scaffolds populated with hFOB 1.19 cells for 24h and 48h as assayed by using cytotoxicity detection kit TOX-7. The absorbances measured at 490 nm are plotted against the culture time period. Statistics performed using one-way ANOVA with Bonferroni's multiple comparison tests show that the results are not statistically significantly different

Behaviour of hFOB 1.19 cells cultured on scaffolds. To assess cellular response, specific staining of actin cytoskeleton, β1 integrin and fibronectin was performed. Fluorescence microscopy images allowed to determine that hFOB 1.19 cells were well adhered to scaffolds after 24 h in culture (Fig. 9). Cell spreading was variable and cells were polygonal or spindle-shaped. Some of them displayed long cytoplasmic extensions, which frequently contacted other cells. Lateral attachment of cells to the inner wall of the pores, was evident at this stage, as well as cells spanning the diameter of the pore. Within 24 h, the polymerized actin long fibbers that extended throughout the entire cell body were clearly visible. Furthermore, there were no evident differences between actin patterns of hFOB 1.19 grown on HAP versus β-TCP and HAP+β-TCP.

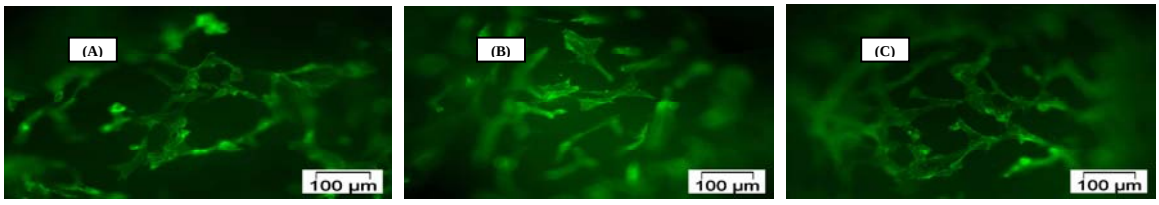

Fig. 9. Fluorescent micrographs of hFOB 1.19 cells growing 24 h inside: (A) HAP; (B) β-TCP; (C) HAP+β-TCP, stained with FITC-conjugated phalloidin to visualize actin cytoskeleton

Because the biologic fixation of implants depends on optimal cell interactions at interface, an objective of this study was to examine the expression of the main partners involved in cell-ECM interactions, namely, β1 integrins and fibronectin. β1 integrin immunofluorescence (Fig. 10) was mostly observed as bright aggregations at the cell periphery and, particularly, at the leading edge of the advancing lamellipodium, contributing to the adherence of the osteoblasts to substrate, forming focal adhesions and mediating their spreading and migration.

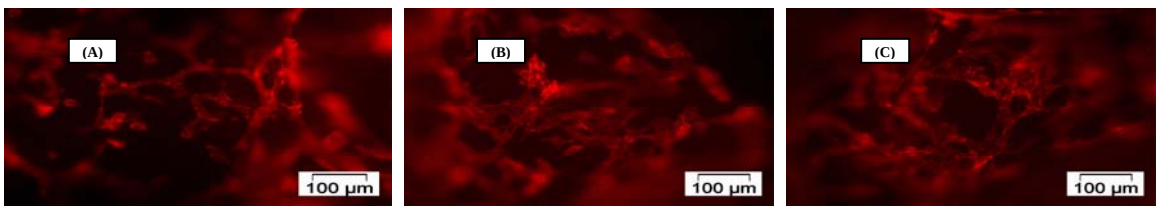

Fig. 10. Integrin β1-subunit expression, assessed by immunofluorescence, in hFOB 1.19 cells cultured for 24h on: (A) HAP; (B) β-TCP; (C) HAP+β-TCP scaffolds

To visualize and compare Fn extracellular network formed as a result of reorganization of Fn adsorbed to and secreted on the three scaffolds seeded with hFOB 1.19 cells, ten days after cell plating these samples were fixed with paraformaldehyde and treated with anti-Fn (mouse) primary antibody, and then incubated with anti-mouse secondary antibody labelled with FITC. The nuclei were counterstained with DAPI to reveal cell density.

Fluorescence images from randomly selected microscopic fields revealed a well organized extracellular Fn-fibrillar network without considerable differences between the analysed scaffolds (Fig. 11). However, slight differences in Fn mesh density depending on cell density were remarked. In samples without primary antibody, there was no Fn matrix seen.

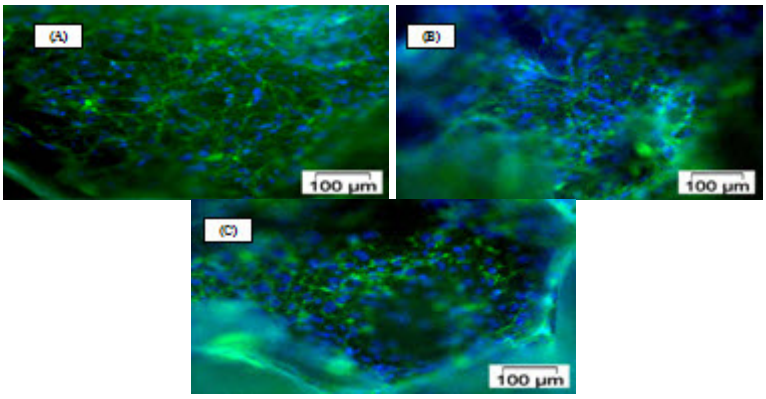

Fig. 11. Immunofluorescence localization of Fn (green) synthesized and assembled into an extracellular fibrillar network by hFOB 1.19 cells grown into: (A) HAP; (B) β-TCP; (C) HAP+β-TCP scaffolds for 10 days

By DAPI staining of nuclei, it was possible to observe the cell colonization both on the surface of the material and in the scaffold inner regions accompanied by Fn production by the cells. At 10 days post-seeding, hFOB 1.19 cells had massively colonized the scaffolds, showing that these substrates adequately promoted cell adhesion and proliferation.

4. Discussion

The scaffold morphology showed a dense polycrystalline structure with cavities (porosity), junctions and interconnections that can facilitate the cell proliferation.

Also, the scaffold porosity varied in normal limits [2] and presented a bimodal and three modal distribution of the pore dimensions. These bimodal and three modal distributions improve [22] the mechanical properties of the scaffolds.

Concerning the weight variations of the studied scaffolds, it can be concluded:

- hydroxyapatite (HAP) presented the increase of its weight i.e., on its surface were deposited calcium and phosphorous ions from SBF; the quantity of the deposited ions increased till 1000 immersion hours, then remained about constantly, namely, the deposition process was equal with the dissolution process.

- β tricalcium phosphate (β-TCP) revealed the loss of its weight, i.e., this scaffold dissolved in SBF; correlating with SEM studies, it appeared that the dissolution process is a little more intensively than the deposition process of calcium and phosphorous ions from SBF;

- hydroxyapatite+β tricalcium phosphate (HAP+β-TCP) exhibited a lower dissolution process than the β-TCP because its weight variations had lower values; however, the deposition process (that takes concomitantly place with the dissolution process) is more intensively than on β-TCP.

The results from Table 3 confirm the fact that simultaneously with the dissolution, on the surface of studied materials were deposited calcium and phosphorous ions, namely, these materials are bioactive and biodegradable, i.e. favourable to the bone formation.

The pH values increased (at the beginning) from the initial value of 7.75 to 8.5 due to the dissolution process of the soluble phases [14]; then, the pH values decreased till about 8.2 – 8.2; after 1000 hours, an about constant level (8.5) was reached; this behaviour can be attributed to the deposition of calcium and phosphorous ions from SBF [14] i.e. to the scaffold bioactivity.

Regarding the decreasing of calcium and phosphorous ion quantity from SBF in time, it was showed [14] that, these ions enter in the scaffold pores and progressively nucleate and crystallise as apatite. This fact was also demonstrated by our SEM studies that revealed that the pores are fully or partially covered by a deposited layer, namely, takes place a process of the new deposited bone in the open structure of the scaffolds.

After 700 immersion hours in SBF, the morpho-structural changes of the surface are explained by the deposition on the walls of an outer thin layer during immersion in SBF. A closer observation of the deposited layer shows that the surfaces are fully covered by a continuous layer of acicular nano-sized grains, hundreds of nm long and tens of nm wide (Fig. 6A-B). It is known that β-TCP tends to crystallize from aqueous solution in the form of acicular grains [14]. The deposition of aggregates of nano-filaments in the β-TCP scaffold (Fig. 6C-D) indicates a higher rate of deposition from SBF on β-TCP than on HAP surfaces.

The aggregates of nano-particles deposited on the HAP, β-TCP and HAP+β-TCP scaffold surfaces, after 2100 h prove an intensive deposition process i.e. the bioactivity of these scaffolds.

The first objective of cell culture assays was to determine if these ceramic scaffolds affected cellular survival. To test this parameter, the LDH activity in the culture media was quantified. As seen in Figure 8, the cells grown in contact with the three analysed substrates proved to display low LDH release in culture medium suggesting that none of them exerted cytotoxic effects. Taking into consideration that in culture, morphology indicates the health status of the cells, fluorescent actin staining with FITC-conjugated phalloidin was realized. This study revealed that osteoblasts with both polygonal and spindle-shaped morphology populated the inner walls of pores (Fig. 9).

Another sensitive indicator for the biocompatibility of implant materials is represented by structural organization of components involved in cell–matrix and cell–cell adhesion. Cell-ECM adhesion is largely mediated by integrin family of transmembrane receptors. Integrins are composed of α and β subunits able to dimerize in specific combinations that both are dependent on and determine the ECM or surface structure on which the receptor binds (e.g., α2β1 for collagen and α5β1 for fibronectin) [31,32]. Integrin expression has been shown to be involved in cell signaling pathways that influence cell survival, proliferation and differentiation [32-34]. We have shown the presence of bright aggregations of β1 integrin at the periphery of spread cells (Fig. 10) that attach the extracellular portion of the cell to the intracellular cytoskeletal portion, essential for signal transduction and then regulation of gene expression and finally cell behaviour. The presence of β1 integrins immunofluorescence at the rest of the main cell body in the hFOB 1.19 cells may be, either, due to non-clustered non-activated integrins where a diffused pattern is observed, or due to the novo-formed clusters of integrin, where immunofluorescent aggregations are displayed.

It is well known that extracellular integrin ligands are not passive adhesive molecules but are active participants in the cell adhesion process such as fibronectin, vitronectin, collagen or laminin [35,36]. These molecules can be adsorbed on the material surface from the surrounding environment, i.e. serum within cell culture media *in vitro* or body fluids *in vivo*, and/or synthesized and extracellularly secreted where they are assembled in an ECM. Extracellular matrix assembly confers the mechanical properties of the new tissue generated at the implant interface.

In the present study, Fn fibrillar matrix was examined by an immunofluorescence assay. Fibronectin is an abundant component of the ECM, secreted by the cells as a soluble dimmer and considered the major molecule mediating cell attachment [37]. It is assembled into an insoluble dense network of interconnected fibrils at the cell surface which provide a dynamic environment for cells. Fn fibril formation depends on the interaction between soluble Fn and integrin receptors on the cell surface [38]. Integrins link Fn fibrils to the actin cytoskeleton and this connection mediates Fn fibril formation and influences the alignment of the Fn fibrils and the cytoskeleton, leading to variations in fibril organisation [38,39]. It has been demonstrated that osteoblasts can synthesize and secrete Fn to form fibril matrix network underneath the cell [40]. The Fn network is

an important factor for cell differentiation, expression of physiological function, and survival of osteoblasts [41].

It is important to mention that this 3D culture system offers difficulties in fluorescence visualization due to the porosity of samples. However, by analysis of the ceramic supports in different microscopic plans we managed to get information about the possibilities to combine the cells with porous scaffolds to produce 3D hybrid constructs useful in bone tissue engineering.

5. Conclusions

1. The new ceramic scaffolds have a porous structure with junctions and interconnections, favourable for cell adhesion and proliferation.
2. The scaffolds revealed very good compression resistance, very close to cancellous bone.
3. Scaffold porosity presented a bimodal or three modal distribution of the pore sizes that improve their mechanical properties.
4. The results confirmed the fact that simultaneously with the dissolution, on the surface of studied materials were deposited calcium and phosphorous ions, namely, these materials are favourable to the bone formation.
6. The quantity of the calcium and phosphorus ions from SBF decreased in the first 1000 immersion hours due to their deposition on the scaffolds; after then, their quantity remained about constantly i.e., the simultaneous processes of dissolution and deposition are compensated, namely, the scaffold dissolution is supplied by the bone formation.
7. The morpho-structural studies confirmed that, after 2100 immersion hours, the scaffolds coated with a layer of nano-sized acicular grains, i.e., the new bone was deposited.
8. The results by LDH assay proved that hFOB 1.19 cells are able to attach, spread, migrate towards the interior of the scaffolds, proliferate, synthesize and extracellularly assemble ECM molecules.
9. All the three analysed scaffolds are favourable environment for hFOB 1.19 cells. These bioceramics have stimulated in different proportions the synthesis of the bone ECM. Thus, the HAP matrices have proved the best osteoinductive potential, being assisted by the β-TCP material and, finally, the composite HAP+β-TCP.

Acknowledgement

This work was supported by Romanian CNCSIS – UEFISCSU, project number PN II – IDEI code 248/2010.

References

[1] V. Bayazit, M. Bayazit, E. Bayazit, Digest J. Nanomater. Biostruct. **5**, 267 (2010).
[2] K. S. Chan, W. Liang, W. L. Francis, D. P. Nocolella, J. Mech. Behav. Biomed. Mater. **3**, 584 (2010).
[3] K. F. Leong, C. K. Chua, N. Sudarmadji, W. Y. Yeong, J. Mech. Behav. Biomed. Mater. **1**, 140 (2008).
[4] J. R. Jones, J. Eur. Ceram. Soc. **29**, 1275 (2009).
[5] M. Kamitakahara, C. Ohtsuki, T. Miyazaki, J. Biomater. Appl. **23**, 197 (2008).
[6] A. Costescu, I. Pasuk, F. Ungureanu, A. Dinischiotu, M. Costache, F. Huneau, S. Galaup, P. Le Coustumer, D. Predoi, Digest J. Nanomater. Biostruct. **5**, 989 (2010).
[7] T. Mygind, M. Stiehler, A. Baatrup, H. Li, X. Zou, A. Flyvbjerg, M. Kassem, C. Bunger, Biomaterials **28**, 1036 (2007).
[8] K. M. Woo, J. H. Jun, V. J. Chen, J. Seo, J. H. Baek, H. M. Ryoo, G. S. Kim, K. J. Somerman, P. X. Ma, Biomaterials **28**, 335 (2007).
[9] M. Descamps, J. C. Hornez, A. Leriche, J. Eur. Ceram. Soc. **29**, 369 (2009).
[10] F. Pecqueux, F. Tancret, N. Payraudeau, J. M. Bouler, J. Eur. Ceram. Soc. **30**, 819 (2010).
[11] H. Nakayama, T. Kawase, H. Kogami, K. Okuda, H. Inoue, T. Oda, K. Hayama, M.

Tsuchimochi, L. F. Wolff, J. Biomater. Appl. **24**, 751 (2010).
[12] S. Shi, X. Cheng, J. Wang, W. Zhang, L. Peng, Y. Zhang, J. Biomater. Appl. **23**, 331 (2009).
[13] F. Zhang, J. Chang, K. Lin, J. Lu, J. Mater. Sci. Mater. Med. **19**, 167 (2008).
[14] S. Sanchez-Salcedo, F. Balas, I. Izquierdo-Barba, M. Valett-Regi, Acta Biomater. **5**, 2738 (2009).
[15] Y. H. Hsu, I. G. Turner, A. W. Miles, J. Mater. Sci. Mater. Med. **18**, 2319 (2007).
[16] Q. Z. Chen, K. Rezwan, V. Francon, D. Armitage, S. N. Nazhat, F. H. Jones, A. R. Boccaccini, Acta Biomater. **3**, 551 (2007).
[17] C. Bergmann, M. Linder, W. Zhang, K. Koczur, A. Kirsten, R. Telle, H. Fischer, J. Eur. Ceram. Soc. **30**, 2563 (2010).
[18] N. Dunne, V. Jack, R. O'Hara, D. Farrad, F. Buchanan, J. Mater. Sci. Mater. Med. **21**, 2263 (2010).
[19] J. Xi, L. Zhang, Z. Zheng, G. Chen, Y. Gong, N. Zhao, X. Zhang, J. Biomater. Appl. **22**, 293 (2008).
[20] L. Jianguo, Z. Li, Z. Yi, W. Huanan, L. Jidong, Z. Qin, Y. Hi, J. Biomater. Appl. **24**, 31 (2009).
[21] G. L. Converse, T. L. Conrad, R. K. Roeder, J. Mech. Behav. Biomed. Mater. **2**, 627 (2009).
[22] T. Takayama, M. Todo, A. Takano, J. Mech. Behav. Biomed. Mater. **2**, 105 (2009).
[23] T. V. Chirila, D. A. Morrison, Z. Gridneva, A. J. A. Garcia, S. T. Plattem, B. J. Zainuddin, A. K. Whittaker, J. P. Hills, J. Mater. Sci. **40**, 4987 (2005).
[24] A. A. Al-Munajed, F. J. O'Brien, J. Mech. Behav. Biomed. Mater. **2**, 138 (2009).
[25] T. Kokubo, T. Matsushita, H. Takadama, T. Kizuki, J. Eur. Ceram. Soc. **29**, 1267 (2009).
[26] S. Liao, R. Murugan, C. K. Chan, S. Ramakrishna, J. Mech. Behav. Biomed. Mater. **1**, 252 (2008).
[27] A. Nocivin, D. Raducanu, I. Cinca, D. Cojocaru, A. Cimpean, F. Grigore, R. Ion, Metallurgia Int. **XIV**, 42 (2009).
[28] E. Vasilescu, P. Drob, D. Raducanu, I. Cinca, D. Mareci, J. M. Calderon Moreno, M. Popa, C. Vasilescu, J. C. Mirza Rosca, Corros. Sci. **51**, 2885 (2009).
[29] M. V. Popa, E. Vasilescu, P. Drob, D. Mareci, J. M. Calderon Moreno, S. Ivanescu, C. Vasilescu, J. C. Mirza Rosca, Mater. Corros. **60**, 949 (2009).
[30] E. Vasilescu, P. Drob, D. Raducanu, V. D. Cojocaru, I. Cinca, D. Iordachescu, R. Ion, M. Popa, C. Vasilescu, J. Mater. Sci. Mater. Med. **21**, 1959 (2010).
[31] R. K. Sinha, R. S. Tuan, Bone **18**, 451 (1996).
[32] T. Saito, S. M. Albelda, C. T. Brighton, J. Orthop. Res. **12**, 384 (1994).
[33] A. K. Shah, R. K. Sinha, N. J. Hickok, R. S. Tua, Bone **24**, 499 (1999).
[34] G. Rh. Owen, D. O. Meredith, I. Gwynn, R. G. Richards, Eur. Cell. Mater. **9**, 85 (2005).
[35] T. Growth, G. Altankov, A. Kostadinova, N. Krasteva, W. Albrecht, D. Paul, J. Biomed. Mater. Res. **44**, 341 (1999).
[36] A. J. Garcia, M. D. Vega, D. Boettiger, Mol. Biol. Cell. **10**, 785 (1999).
[37] K. M. Yamada. "Fibronectin domains and receptors", in: D. E. Mosher, (Ed.), Fibronectin, New York and London, Academic Press Inc., pp. 48-121 (1989).
[38] I. Wierzbicka-Patynowski, J. E. Schwarzbauer, J. Cell. Sci. **116**, 3269 (2003).
[39] C. Wu, V. M. Keivens, T. E. O'Toole, J. A. McDonald, M. H. Ginsberg, Cell **83**, 715 (1995).
[40] R. S. Yang, C. H. Tang, Q. D. Ling, S. H. Liu, V. M. Fu, Mol. Pharmaco. **l61**, 1163 (2002).
[41] R. K. Globus, S. B. Doty, J. C. Lull, J. Cell. Sci. **111**, 1385 (1998).